PHYSICS AND CHEMISTRY OF SOLIDSTATE
V. 18, № 1 (2017) P. 122-128
DOI: 10.15330/pcss.18.1.122-128

ФІЗИКА І ХІМІЯ ТВЕРДОГО ТІЛА
Т. 18, № 1 (2017) С. 122-128

PACS: 539.213.27

ISSN 1729-4428

L. Boichyshyn, M.-O. Danyliak, B. Kotur, T. Mika[1]

The Kinetic Peculiarities of the Nanocrystallization of Amorphous Alloys $Fe_{84}Nb_2B_{14}$, which are Doped by Rare Earth Metals

Ivan Franko National University of Lviv, Kyryla and Mefodia St. 6, 79005 Lviv, Ukraine, lboichyshyn@yahoo.com
[1]Institute for Metal Physics of NAS of Ukraine, 36 Vernadsky St., Kyiv 03142, Ukraine

The thermal stability and crystallization of the $Fe_{82}Nb_2B_{14}RE_2$ (RE = Y, Gd, Tb, Dy) amorphous alloys were investigated by differential scanning calorimetric (DSC) method. By X-ray diffraction (XRD) method has been established that the initial AMA have amorphous structure. The RE alloying of $Fe_{82}Nb_2B_{14}RE_2$ amorphous alloys increase the nanocrystallization temperatures for ~ 110 K and activation energies of crystallization for ~ 330 kJ/mol. The Avrami constant was found to be 1.86 for $Fe_{84}Nb_2B_{14}$ at 703 K, 1.17 for $Fe_{82}Nb_2B_{14}Y_2$ at 813 K, 1.36 for $Fe_{82}Nb_2B_{14}Gd_2$ at 808 K, 1.76 for $Fe_{82}Nb_2B_{14}Tb_2$ at 808 K and 1.92 for $Fe_{82}Nb_2B_{14}Dy_2$ at 808 K. Two-dimensional diffusion controlled growth mechanism with decreasing nucleation rate was observed in the alloys.

Keywords: Amorphous alloys; Crystallization; Kinetics models; Activation energy.

Article acted received 22.11.2016; accepted for publication 05.03.2017.

Introduction

Due to the lack of crystal structure, amorphous metallic alloys (AMA) possess high strength and elasticity, superior corrosion resistance and excellent wear resistance [1]. Amorphous and nanocrystalline alloys based on iron obtained by melt spinning technique widely used as soft magnetic materials [2, 3]. Amorphous alloys are widely used as precursors of nanostructured materials. Using an appropriate thermal annealing at temperatures close to the crystallization temperature one can obtain a microstructure with iron nanograins embedded in an amorphous matrix. Soft magnetic properties of amorphous alloys are found to be superior to those of conventional materials [4].

The key to the formation of nanocrystallites in an amorphous alloy of a suitable chemical composition is to control the annealing temperature and time to ensure relatively high nucleation rate and a low growth rate. It is already known that the crystallization (nanocrystallization) kinetic depends on chemical composition of the alloy [2, 4]. Addition of a transition metal (Nb, Zr, Hf etc) during crystallization process stabilizes an amorphous phase and inhibits a grain growth. Transition elements have also a notable effect on magnetic properties of the amorphous and nanocrystallied Fe-based alloys [5, 6].

Some investigations have been performed on effects of rare earth (RE) addition on the thermal stability and crystallization kinetics of Fe-based amorphous alloys. For example, in work [7] examined thermal stability and crystallization behavior of $(Fe_{0.75-x}Dy_xB_{0.2}Si_{0.05})_{96}Nb_4$ (x = 0 - 0.07) bulk metallic glasses. The thermal stability of the amorphous $(Fe_{0.75-x}Dy_xB_{0.2}Si_{0.05})_{96}Nb_4$ was greatly improved by alloying with a small amount of Dy (x = 0 - 0.07). The activation energy for the nanocrystallization peak increased with the addition of Dy. However, by adding more Dy one can restrain the precipitation of α-Fe and change primary precipitation phase from $Fe_{23}B_6$ phase into $DyFe_{11}Si$ and $DyFe_3$ phases.

Influence of composition in the crystallization process of $Fe_{75-x}Nb_{10}B_{15+x}$ metallic glasses was studied too [8]. In the first two alloys $Fe_{23}B_6$ is obtained as the main primary crystallization product, whereas in $Fe_{75}Nb_{10}B_{15}$ alloy α-Fe is obtained. Furthermore, in $Fe_{75}Nb_{10}B_{15}$ alloy process occurs in two steps without obtaining a significant amount of $Fe_{23}B_6$. These facts retard the precipitation of the Fe_3B phase to higher temperatures in $Fe_{75}Nb_{10}B_{15}$ than in $Fe_{65}Nb_{10}B_{25}$–$Fe_{70}Nb_{10}B_{20}$ alloys.

Crystallization mechanisms have been effectively evaluated using kinetic models (Kissinger, Ozawa, and Matusita) and differential scanning calorimetric (DSC) method. Furthermore, activation energy of crystallization, Avrami exponent, and growth mechanisms can be examined by using the mentioned models [9]. Kissinger peak method was widely used to determine activation energies in the reactions when the

temperatures of peaks cannot be determined accurately due to overlapping heat effects. On the other hand,

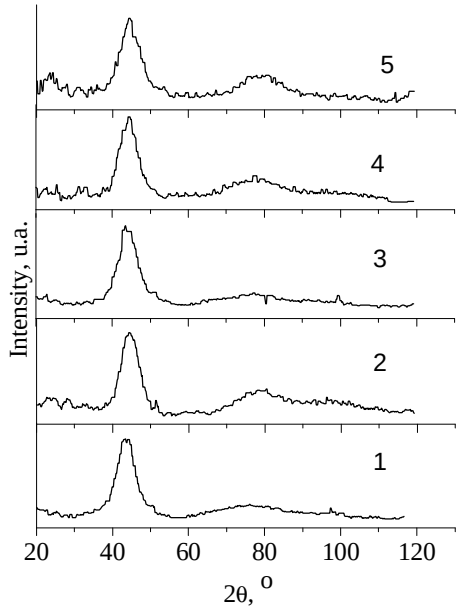

Fig 1. XRD patterns of the initial samples: 1 - $Fe_{84}Nb_2B_{14}$, 2 - $Fe_{82}Nb_2B_{14}Y_2$, 3 - $Fe_{82}Nb_2B_{14}Gd_2$, 4 - $Fe_{82}Nb_2B_{14}Tb_2$, 5 - $Fe_{82}Nb_2B_{14}Dy_2$.

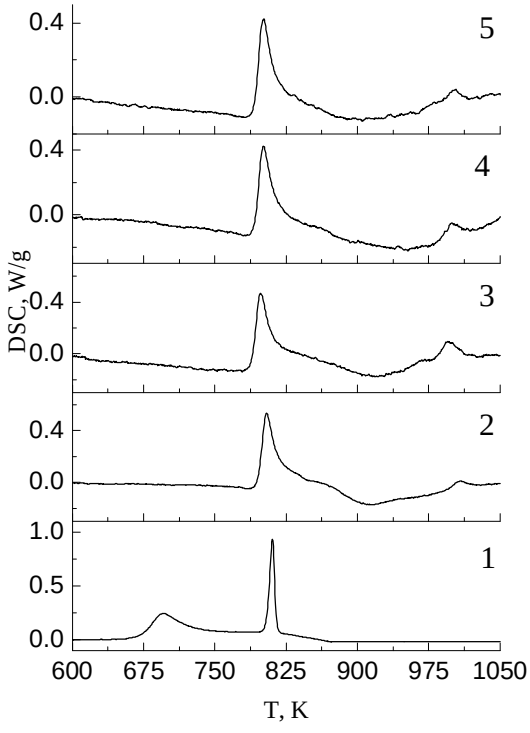

Fig. 2. DSC thermograms of Fe-Nb-B-RE alloys with different rare earth alloying additions: 1 - $Fe_{84}Nb_2B_{14}$, 2 - $Fe_{82}Nb_2B_{14}Y_2$, 3 - $Fe_{82}Nb_2B_{14}Gd_2$, 4 - $Fe_{82}Nb_2B_{14}Tb_2$, 5 - $Fe_{82}Nb_2B_{14}Dy_2$ (heating rate 10

Avrami exponent and growth mechanisms can be investigated using Matusita model. For example, characterization of crystallization process in Fe-based magnetic amorphous alloys such as $(Fe_{50}Co_{50})_{73.5}Ag_1Nb_3Si_{13.5}B_9$, $Fe_{75}Si_9B_{16}$, and $Fe_{83}B_{17}$ has shown a diffusion controlled growth mechanism and two step crystallization mechanism [6].

In our earlier investigation [10] it was shown the crystallization of the $Fe_{82}Nb_2B_{14}RE_2$ (RE = Y, Gd, Tb and Dy) amorphous alloys proceeds in two stages. The RE alloying additions cause a slowing down of diffusion processes i.e. increase the temperature of primary crystallization for ~ 110 K in comparison with the basic $Fe_{84}Nb_2B_{14}$ alloy and accelerate nucleation fine-grained nanostructures of α-Fe and $Fe_{23}B_6$ phases with mean crystallites size of 15 - 19 nm.

In this paper, we report a study of kinetics of crystallization and effects of RE (RE = Y, Gd, Tb, Dy) alloying on the nucleation of crystalline phases in $Fe_{82}Nb_2B_{14}RE_2$ amorphous alloys. The alloy $Fe_{84}Nb_2B_{14}$ was also examined as the basic one (reference alloy).

I. Experimental

Amorphous alloys: $Fe_{84}Nb_2B_{14}$, $Fe_{82}Nb_2B_{14}Y_2$, $Fe_{82}Nb_2B_{14}Gd_2$, $Fe_{82}Nb_2B_{14}Tb_2$ and $Fe_{82}Nb_2B_{14}Dy_2$ obtained by melt spinning technique in helium atmosphere onto a copper wheel with a circumferential speed of about 30 m/s. The obtained amorphous alloys were in the form of strips with thickness and width of 20–25 μm and 3 mm, respectively. The melt was prepared from pure Fe and B and binary $REFe_2$ (RE = Y, Gd, Tb, and Dy) and $NbFe_2$ compounds. Purity (wt. %) of the initial elements was the following: Fe – 99,99; B – 99,96; Y – 99,96; Gd – 99,96; Tb – 99,96 та Dy – 99,96.

Crystallization of the obtained alloys was investigated by differential scanning calorimetry (DSC, NETZSCH DSC 404) method. The samples were heated up to 1050 K with different constant heating rate (β) 5, 10, 20 and 40 K/min. Using the X'Pert Philips Diffractometer PW 3040/60 type with the CuKα-radiation and the X'Cellerator counter diffraction patterns of the initial AMA was obtained.

II. Results and Discussion

In Fig. 1 XRD patterns of the initial alloys (after melt-spinning process) are presented. They show broad diffraction peaks. No peaks corresponding to crystalline phases are detected, which means fully amorphous structures were formed in the samples after melt-spinning process.

The amorphous alloys were scanned in DSC tests at 5, 10, 20, and 40 K/min heating rates. Fig. 2 shows the DSC curves for the investigated alloys. Two peaks are observed in all thermograms showing two-stage (X_1 and X_2) crystallization process in the alloys. DSC thermograms of $Fe_{82}Nb_2B_{14}Gd_2$ alloy for four different heating rates are presented in Fig. 3. It is seen the peak temperatures (T_{X1}, T_{X2}) increase with increasing heating rate and this suggests that crystallization of amorphous

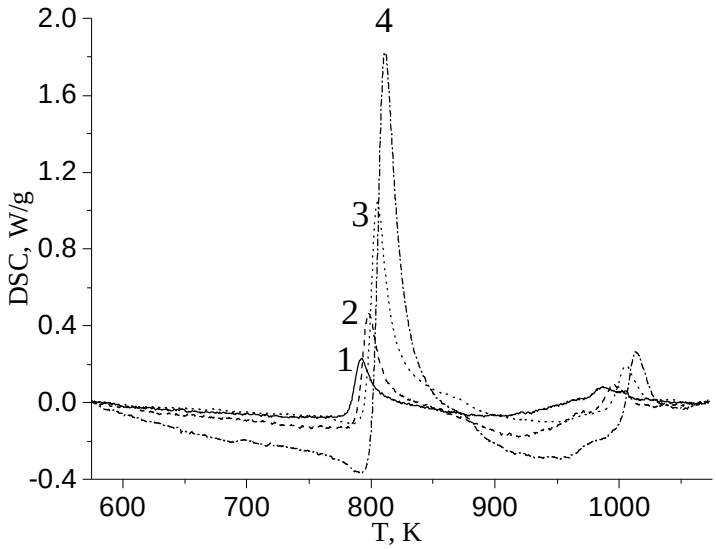

Fig. 3. DSC thermograms of $Fe_{82}Nb_2B_{14}Gd_2$ alloy for four different heating rates: 1 – 5K/min; 2 – 10 K/min; 3 – 20 K/min; 4 – 40 K/min.

Table 1

T_{X1} and T_{X2} for four different heating rates (β) of the alloys

Alloys	T_{X1}, K				T_{X2}, K			
	β							
	5 K/min	10 K/min	20 K/min	40 K/min	5 K/min	10 K/min	20 K/min	40 K/min
$Fe_{84}Nb_2B_{14}$	684	696	708	719	802	811	821	830
$Fe_{82}Nb_2B_{14}Y_2$	798	804	811	818	995	1008	1016	1023
$Fe_{82}Nb_2B_{14}Gd_2$	793	798	806	811	986	995	1006	1013
$Fe_{82}Nb_2B_{14}Tb_2$	795	801	808	815	1000	1000	1008	1016
$Fe_{82}Nb_2B_{14}Dy_2$	794	801	808	814	991	1000	1007	1017

phase depends on atoms diffusion speed. Table 1 shows the changes in the first (T_{X1}) and second (T_{X2}) crystallization peaks with increasing heating rate for $Fe_{84}Nb_2B_{14}$, $Fe_{82}Nb_2B_{14}Y_2$, $Fe_{82}Nb_2B_{14}Gd_2$, $Fe_{82}Nb_2B_{14}Tb_2$ and $Fe_{82}Nb_2B_{14}Dy_2$ alloys. The crystallization temperatures T_{X1} and T_{X2} significantly increase with RE alloying of the initial alloy $Fe_{84}Nb_2B_{14}$. The temperatures of crystallization peaks of the $Fe_{82}Nb_2B_{14}Y_2$ amorphous alloy are higher compared to the other alloys (Table 1).

Kissinger peak method and Ozawa model were used to determine the activation energy, E_a, in the first step of crystallization. According to Kissinger model (Eq. (1)):

$$\ln\frac{T^2}{b} = \frac{E_a}{T_X R} + A \qquad ,(1)$$

where: β is heating rate, E_a – activation energy, R is the gas constant, T_X is the peak temperature and A – constant, plotting $\ln(T_X^2/\beta)$ *vs* $1000/T_X$ gives a straight line and the slope of it equals $-E_a/R$ [11]. Kissinger plots for the examined amorphous alloys are presented in Fig. 4.

Activation energy for the first step of crystallization for the $Fe_{84}Nb_2B_{14}$, $Fe_{82}Nb_2B_{14}Y_2$, $Fe_{82}Nb_2B_{14}Gd_2$, $Fe_{82}Nb_2B_{14}Tb_2$, $Fe_{82}Nb_2B_{14}Dy_2$ alloys was calculated to be 232, 567, 581, 561, 543 kJ/mol, respectively.

$$\ln b = -\frac{E_a}{RT_X} + B, \qquad (2)$$

where: B is constant for investigated alloys, was also used for calculation of activation energy for the first crystallization peak of the alloys. In this model, plotting $\ln\beta$ vs $1/T_X$ gives a straight line and slope of a line equals to $-E_a/R$ [12].

$\ln\beta$ as a function of $1000/T_X$ for the first endothermic heat effect for investigated alloys are shown in Fig. 5. Activation energy for nanocrystallization phases in the $Fe_{84}Nb_2B_{14}$, $Fe_{82}Nb_2B_{14}Y_2$, $Fe_{82}Nb_2B_{14}Gd_2$, $Fe_{82}Nb_2B_{14}Tb_2$, $Fe_{82}Nb_2B_{14}Dy_2$ alloys was calculated to be 245, 580, 595, 575, 557 kJ/mol, respectively. The E_a values received by Kissinger model are slightly decreased while comparing for the same data calculated by Ozawa method, but the differences between the values determined by the two methods are ~ 3–6 %. Similar results were received by the authors of Refs. [13–15] when they studied crystallization kinetics of $Fe_{95}Si_5$, $Zr_{70}Cu_{20}Ni_{10}$ and $Fe_{89.8}Ni_{1.5}Si_{5.2}B_3C_{0.5}$ metallic glasses.

RE alloying for only 2 at. % of the basic $Fe_{84}Nb_2B_{14}$ alloy causes significant increase of nanocrystallization

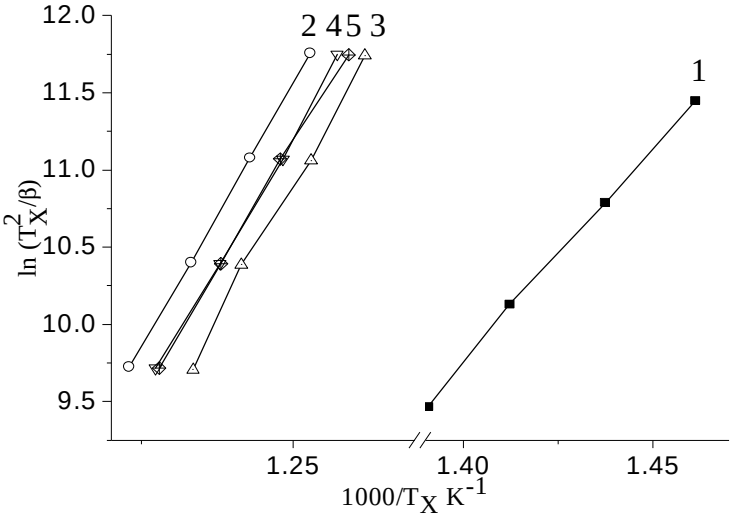

Fig. 4. Kissinger plots for the examined amorphous alloys: 1 - $Fe_{84}Nb_2B_{14}$, 2 - $Fe_{82}Nb_2B_{14}Y_2$, 3 - $Fe_{82}Nb_2B_{14}Gd_2$, 4 - $Fe_{82}Nb_2B_{14}Tb_2$, 5 - $Fe_{82}Nb_2B_{14}Dy_2$.

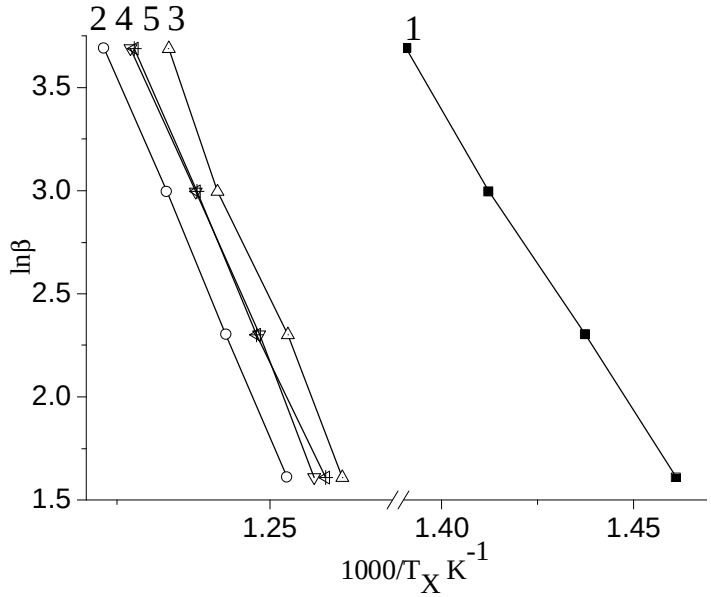

Fig. 5. lnβ as a function of 1000/T_X for the first crystallization step in the 1 – $Fe_{84}Nb_2B_{14}$, 2 – $Fe_{82}Nb_2B_{14}Y_2$, 3 – $Fe_{82}Nb_2B_{14}Gd_2$, 4 – $Fe_{82}Nb_2B_{14}Tb_2$, 5 – $Fe_{82}Nb_2B_{14}Dy_2$ alloys according to Ozawa model.

temperatures and activation energies of nanocrystallization of the $Fe_{82}Nb_2B_{14}RE_2$ amorphous alloys.

The volume fraction of transformed structure from amorphous to crystalline state can be obtained from DSC thermograms. At each temperature, volume fraction of crystalline phases (α) can be estimated according to Eq. (3):

$$a = \frac{S_i}{S_T}, \qquad (3)$$

where S_T is the total area of the exothermic peak and S_i is the area between the initial point of the peak and any other temperature [12].

In Fig. 6 the plot of α vs T at different heating rates is shown for the first step of crystallization for the initial and the Dy containing alloys.

All the curves are of sigmoid shape. Minic et al. [16] interpreted this kind of fraction curves as diffusion controlled during crystallization.

To indicate the exact mechanisms of crystal phase growth in the alloys, Matusita model was used (Eq. (4), [9]):

$$\ln\left[-\ln\left(1-a\right)\right] = -n\ln\left(b\right) - 1.052\frac{mE_a}{RT} + C, \quad (4)$$

where α is the volume fraction of crystalline phases, n is Avrami exponent, m is dimensionality of growth, T is temperature and C is constant. In this research, by plotting ln[−ln(1−α)] vs lnβ at constant temperature, Avrami exponent was estimated. Furthermore, by plotting ln[−ln(1−α)] vs reciprocal temperature (1/T) at constant heating rate (β), dimensionality growth parameter (m) was derived. Fig. 7 shows variation of ln[−ln(1−α)] vs lnβ at constant temperature for all investigation alloys. Variation of ln[−ln(1−α)] vs 1/T at constant heating rate (β) for $Fe_{84}Nb_2B_{14}$ and

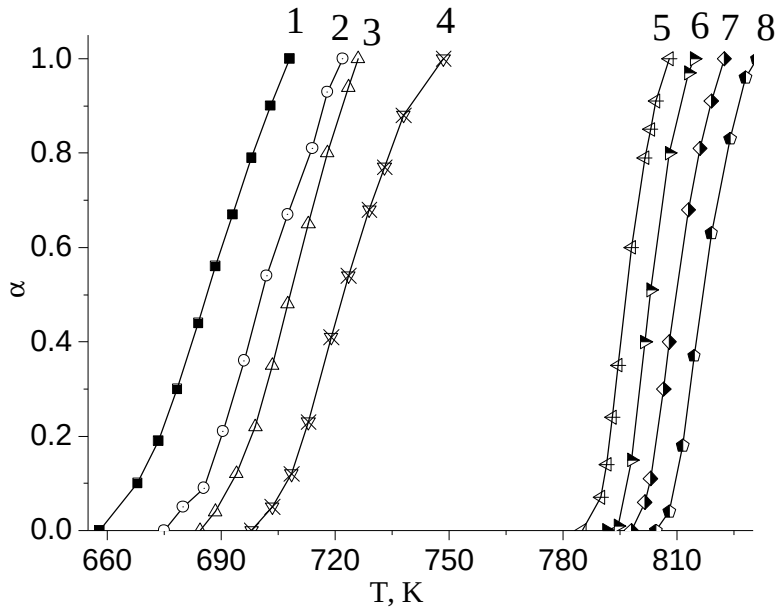

Fig. 6. Fraction of crystallization (α) as a function of temperature at four different heating rates for the $Fe_{84}Nb_2B_{14}$ (1 – 5 K/min; 2 – 10 K/min; 3 – 20 K/min; 4 – 40 K/min) and $Fe_{82}Nb_2B_{14}Dy_2$ (5 – 5 K/min; 6 – 10 K/min; 7 – 20 K/min; 8 – 40 K/min) amorphous alloys.

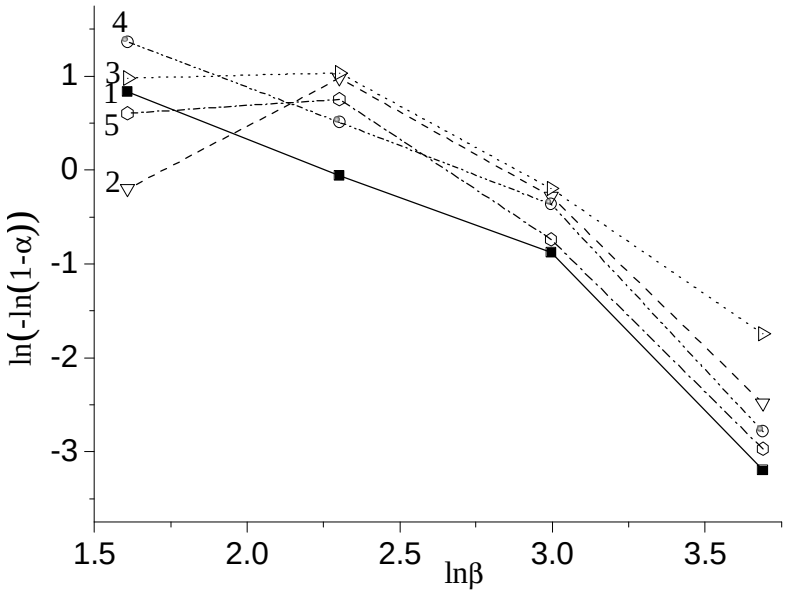

Fig. 7. $\ln[-\ln(1-\alpha)]$ as a function of $\ln\beta$ in constant temperature for the alloys: 1 – $Fe_{84}Nb_2B_{14}$ at 703 K, 2 – $Fe_{82}Nb_2B_{14}Y_2$ at 813 K, 3 – $Fe_{82}Nb_2B_{14}Gd_2$ at 808 K, 4 – $Fe_{82}Nb_2B_{14}Tb_2$ at 808 K, 5 – $Fe_{82}Nb_2B_{14}Dy_2$ at 808 K.

$Fe_{82}Nb_2B_{14}Dy_2$ is plotted in Fig. 8.

Matusita model differs from Kissinger method and it provides valuable information about the Avrami exponent and dimensionality of growth in crystallization of amorphous alloys. In fact, in addition to activation energy, mechanisms of growth can be examined using this method. In general, Avrami exponent (n) can be evaluated according to Eq. (5) [17]:

$$n = b + pm, \qquad (5)$$

where b is a parameter showing nucleation rate, and p is a parameter showing type of transformation, e.g. diffusion controlled transformations. In Table 2 explanations of these parameters are given. The amount of Avrami exponent (n) in this research was calculated to be 1.86 for $Fe_{84}Nb_2B_{14}$ at 703 K, 1.17 for $Fe_{82}Nb_2B_{14}Y_2$ at 813 K, 1.36 for $Fe_{82}Nb_2B_{14}Gd_2$ at 808 K, 1.76 for $Fe_{82}Nb_2B_{14}Tb_2$ at 808 K and 1.92 for $Fe_{82}Nb_2B_{14}Dy_2$ at 808 K alloys.

In effect, the average of dimensionality growth parameter (m = 2) can be inferred from the slopes of straight lines in Fig. 8. It is thought that devitrification process in $Fe_{82}Nb_2B_{14}RE_2$ was carried out by a bulk crystallization mechanism in two dimensions. As mentioned earlier, it can be inferred from Fig. 7 that diffusion controlled crystallization process is accomplished in the alloy and thus, the amount of p is considered equal to 0.5, i. e. parabolic growth of crystal

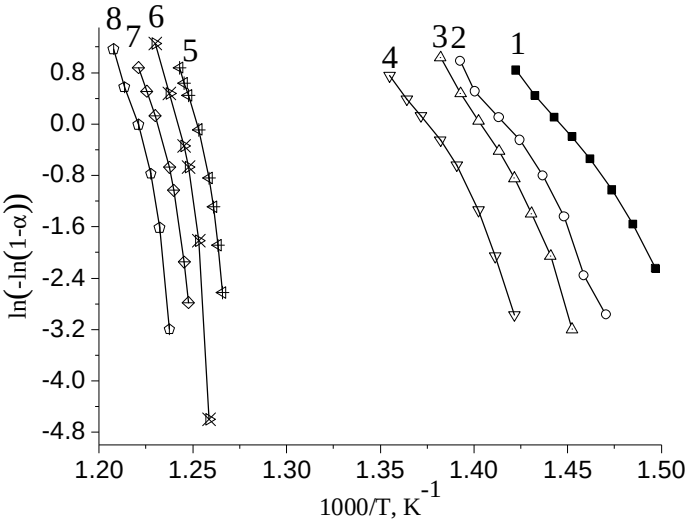

Fig. 8. Matusita plots at different temperatures and heating rates for the $Fe_{84}Nb_2B_{14}$ (1 – 5 K/min; 2 – 10 K/min; 3 – 20 K/min; 4 – 40 K/min) and $Fe_{82}Nb_2B_{14}Dy_2$ (5 – 5 K/min; 6 – 10 K/min; 7 – 20 K/min; 8 – 40 K/min) amorphous alloys.

Table 2

Explanation of nucleation and growth parameters for Eq. 5 [9, 17]

Parameter	Amount	Explanation
m	1	One-dimensional growth mechanism
	2	Two-dimensional growth mechanism
	3	Three-dimensional growth mechanism
p	1	Linear growth (interfacial control)
	0.5	Parabolic growth (diffusion control)
b	>1	Increasing nucleation rate
	0	No nucleation during crystallization (this means that all nuclei may be present before devitrification)
	<1	Decreasing nucleation rate

(see Table 2). Resulting from Eq. (5) and the values of growth parameters, a decreasing nucleation rate is probable for nanocrystallization during annealing process of $Fe_{84}Nb_2B_{14}$, $Fe_{82}Nb_2B_{14}Y_2$, $Fe_{82}Nb_2B_{14}Gd_2$, $Fe_{82}Nb_2B_{14}Tb_2$, $Fe_{82}Nb_2B_{14}Dy_2$.

Conclusions

A two-step crystallization process was observed in $Fe_{82}Nb_2B_{14}RE_2$ (RE = Y, Gd, Tb, Dy) amorphous alloys. The first stage occurs at ~ 696 K (β = 10 K/min) for the basic $Fe_{84}Nb_2B_{14}$ amorphous alloy. Thermal stability ($\Delta E_a \approx 330$ кДж/моль, $\Delta T \approx 110$ K) of the alloys can be significantly increased by addition of only 2 at. % RE.

Activation energy for the crystallization of the nanophases (α-Fe+$Fe_{23}B_6$) was calculated to be 232, 567, 581, 561, 543 kJ/mol for $Fe_{84}Nb_2B_{14}$, $Fe_{82}Nb_2B_{14}Y_2$, $Fe_{82}Nb_2B_{14}Gd_2$, $Fe_{82}Nb_2B_{14}Tb_2$, $Fe_{82}Nb_2B_{14}Dy_2$ alloys, respectively, according to Kissinger model. The values of E_a equal to 245, 580, 595, 575, 557 kJ/mol for $Fe_{84}Nb_2B_{14}$, $Fe_{82}Nb_2B_{14}Y_2$, $Fe_{82}Nb_2B_{14}Gd_2$, $Fe_{82}Nb_2B_{14}Tb_2$, $Fe_{82}Nb_2B_{14}Dy_2$ alloys respectively were calculated according to Ozawa model.

Avrami exponent was measured to be 1.86 for $Fe_{84}Nb_2B_{14}$ at 703 K, 1.17 for $Fe_{82}Nb_2B_{14}Y_2$ at 813 K, 1.36 for $Fe_{82}Nb_2B_{14}Gd_2$ at 808 K, 1.76 for $Fe_{82}Nb_2B_{14}Tb_2$ at 808 K and 1.92 for $Fe_{82}Nb_2B_{14}Dy_2$ at 808 K alloys in the first step of crystallization.

A two-dimensional diffusion controlled growth mechanism with decreasing nucleation rate is probable for devitrification of $Fe_{84}Nb_2B_{14}$, $Fe_{82}Nb_2B_{14}Y_2$, $Fe_{82}Nb_2B_{14}Gd_2$, $Fe_{82}Nb_2B_{14}Tb_2$, $Fe_{82}Nb_2B_{14}Dy_2$ alloys.

Boychyshyn L.M.-Ph.D., Ass.Prof.of the Physical and Colloidal Chemistry Chair;
Danylyak O.M.–Ph.D.-studentof the Physical and Colloidal Chemistry Chair;
Kotur B.Y.–Dr.Chem.Sci.,Professor of the Inorganic Chemistry Chair;
Mika T.M.-Ph.D., young researcher.

[1] G. Wang, Zh. Huang, P. Xiao, X. Zhu, J. Manuf. Process 22, 34 (2016).
[2] M. Karolus, P. Kwapuliński, D. Chrobak, G. Haneczok, A. Chrobak, J. Mater. Process. Tech. 162-163, 203 (2005).
[3] M. Hasiak, W.H. Ciurzyńska, Y. Yamashiro, Mater. Sci. Eng. 261-266, A 293 (2000).
[4] A. Chrobak, D. Chrobak, G. Haneczok, P. Kwapuliński, Z. Kwolek, M. Karolus, Mater. Sci. Eng. A 382, 401 (2004).
[5] J. Torrens-Serra, S. Roth, J. Rodriguez-Viejo, M.T. Clavaguera-Mora, J. Non-Cryst. Solids 354, 5110 (2008).
[6] S. Ahmadi, H.R. Shahverdi, M. Afsari, A. Abdollah-zadeh, J. Non-Cryst. Solids 365, 47 (2013).
[7] J. Li, W. Yang, M. Zhang, G. Chen, B. Shen, J. Non-Cryst. Solids 365, 42 (2013).
[8] J. Torrens-Serra, J. Rodriguez-Viejo, M.T. Clavaguera-Mora, J. Non-Cryst. Solids 353, 842 (2007).
[9] S. Ahmadi, H.R. Shahverdi, S.S. Saremi, J. Mater. Sci. Technol. 27(8), 735 (2011).
[10] A. Chrobak , V. Nosenko, G. Haneczok, L. Boichyshyn, M. Karolus, B. Kotur, J. Non-Cryst. Solids 357, 4 (2011).
[11] I.C. Rho, C.S. Yoon, C.K. Kim, T.Y. Byun, K.S. Hong, Mater. Sci. Eng. B96, 48 (2002).
[12] S. Ahmadi, H.R. Shahverdi, S.S. Saremi, J. Mater. Sci. Technol. 27(6), 497 (2011).
[13] A. Frączyk, Techn. Sc. 14(1), 93 (2011).
[14] H.R. Wang, Y.L. Gao, Y.F. Ye, G.H. Min, Y. Chen, X.Y. Teng, J. Alloys Compd. 353, 200 (2003).
[15] D.M. Minić, A. Gavrilović, P. Angerer, D.G. Minić, A. Maričić, J. Alloys Compd. 482, 502 (2009).
[16] D.M. Minić, A. Maričić, B. Adnadević, J. Alloys Compd. 473, 363 (2009).
[17] S. Ahmadi, H.R. Shahverdi, S.S. Saremi, Iran. J. Mater. Sci. Eng. 7(4), 25 (2010).

Л.М. Бойчишин, М.-О.М. Даниляк, Б.Я. Котур, Т.М. Міка[1]

Кінетичні особливості нанокристалізації аморфних сплавів $Fe_{84}Nb_2B_{14}$, легованих рідкісноземельними металами

Львівський національний університет імені Івана Франка, вул. Кирила і Мефодія 6, 79005 Львів, Україна, lboichyshyn@yahoo.com
[1]Інститут металофізики ім. Г. В. Курдюмова НАН України, бульвар Академіка Вернадського 36, 03142 Київ, Україна, mikat@ukr.net

Методом диференціальної скануючої калориметрії (ДСК) вивчено термічну стабільність і кристалізацію аморфних металевих сплавів (АМС) $Fe_{82}Nb_2B_{14}RE_2$ (RE = Y, Gd, Tb, Dy). Методом рентгенівської дифракції (XRD) встановлено, що вихідні АМС є аморфними. Легування базового АМС $Fe_{84}Nb_2B_{14}$ рідкоземельним металом (RE) спричинило збільшення температури їх нанокристалізації на ~ 110 К та енергії активації кристалізації на ~ 330 кДж/моль. Показник Аврамі для $Fe_{84}Nb_2B_{14}$ становить 1,86 при 703 К, для $Fe_{82}Nb_2B_{14}Y_2$ – 1,17 при 813 К, для $Fe_{82}Nb_2B_{14}Gd_2$ – 1,36 при 808 К, для $Fe_{82}Nb_2B_{14}Tb_2$ – 1,76 при 808 К і 1,92 для $Fe_{82}Nb_2B_{14}Dy_2$ при 808 К. Для досліджених АМС характерним є двовимірний механізм росту кристалічних фаз, зумовлений дифузією атомів зі зменшенням швидкості нуклеації фаз.

Ключові слова: аморфні металеві сплави; кристалізація; кінетичні моделі; енергія активації.